DOI 10.1007/s11204-018-9540-2
Soil Mechanics and Foundation Engineering, Vol. 55, No. 5, November, 2018 (Russian Original No. 5, September-October, 2018)

SOIL MECHANICS

NONLINEAR ANALYSIS OF TUNNEL DEFORMATION AND MECHANISMS OF STRESS TRANSFER CAUSED BY BASEMENT EXCAVATION

UDC 624.131.5/624.191.04

H. S. Sun, L. W. Wang, Y. D. Chen, Y. Dong, J. H. Zhang, and W. B. Sun
Huaiyin Institute of Technology, Huaian, China.

Many new excavations are planned and constructed near or parallel to existing tunnels. Adjacent excavations may significantly impact the stress and deformation of existing tunnels. To evaluate deformation and the mechanisms of stress transfer, well-instrumented centrifuge model tests are back-analyzed using an advanced nonlinear constitutive model, known as a hypoplasticity model. Three-dimensional stress transfer mechanisms along the tunnel axis are demonstrated by changes in normal stresses in the soil around the tunnel. It is found that, for an existing tunnel located directly beneath the basement, the maximum reduction of earth pressure around the tunnel is about 50% at the crown and 20% at the springline of its initial earth pressure. As a result, the tunnel is vertically elongated and horizontally compressed. A tunnel, located at the side of a basement, is elongated along the connection between the right shoulder and left knee and compressed between the left shoulder and right knee. It is expected that this study will help improve the fundamental understanding of three-dimensional stress transfer during basement excavation around existing tunnels.

Introduction

Rapid urban development tends to create a need for construction and engineering projects that may excavate or build close to, or directly above, existing tunnels. Such excavations may cause changes in stresses and deformation of the tunnel lining, not only in a transverse direction but also longitudinally. To investigate the basement-tunnel interaction, a number of field studies have been carried out [1, 2], as well as numerical simulations [3-8] and centrifuge model tests [9-11]. Parameters considered in these studies have included excavation geometry, distance between tunnel and excavation, construction measures, and physical parameters such as sand density, wall stiffness, and tunnel stiffness. Ng et al. [12] considered that numerical methods play an important role in effective modeling and thus compared three constitutive models based on a well-instrumented centrifuge model tests reported previously [9]. It has been found that the hypoplasticity model yields the best predictions of tunnel heave compared with other models such as linear elastic-plastic models that incorporate Mohr-Coulomb failure or the Duncan-Chang model.

Although the effect of basement excavation on adjacent tunnels has been studied by various methods, three-dimensional behavior is not fully understood. This is reflected in the deformation and stress transfer mechanism during the interaction of excavation and an adjacent tunnel.

In this paper, three-dimensional numerical back-analysis is conducted using an advanced constitutive model known as a hypoplasticity model. This modeling is carried out to evaluate deformation and the stress transfer mechanisms during the excavation-soil-tunnel interaction process. The methodology is based on two well instrumented centrifuge model tests conducted by Ng et al. [9]. In the first test pre-

Translated from Osnovaniya, Fundamenty i Mekhanika Gruntov, No. 5, p. 7, September-October, 2018.
0038-0741/18/5505-0298

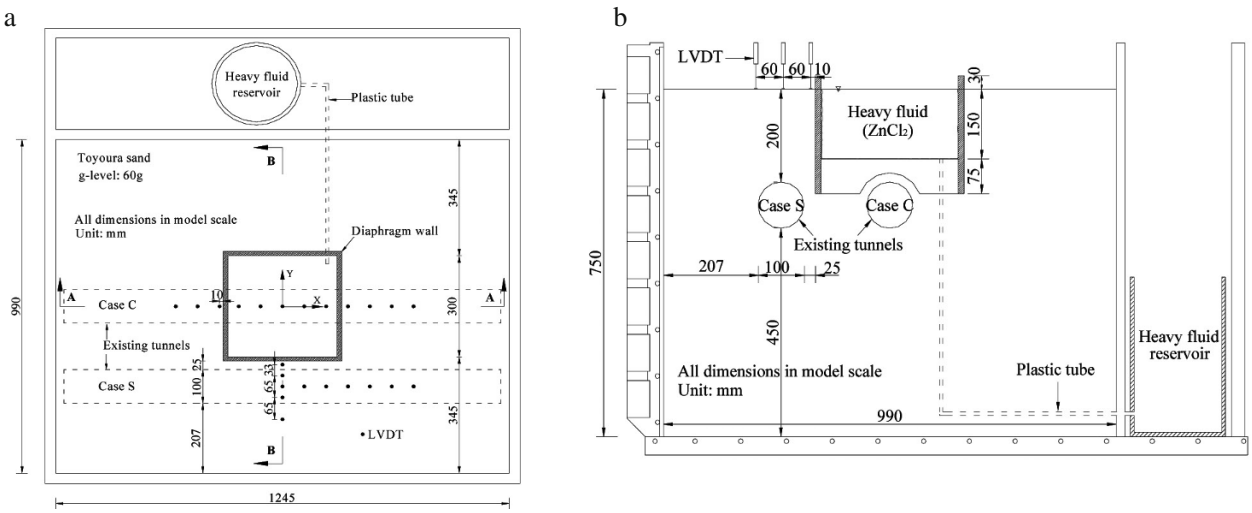

Fig. 1. Centrifuge model tests layout: a) plan view; b) elevation view.

sented in this paper (Case C), an existing tunnel is located directly beneath the basement, while in the second test (Case S), the tunnel is located at the side of the basement. The objectives of these analyses are to improve the fundamental understanding of three-dimensional stress transfer mechanisms during the interaction of excavation and existing tunnel, investigate the different deformation mechanisms for Cases C and S, and identify the zone of influence around an existing tunnel after basement excavation.

Centrifuge Experiments

The layout of the two centrifuge model tests is shown in Fig. 1a. Case C was designed to study the performance of an existing tunnel subjected to basement excavation with the tunnel located directly beneath the basement. Case S, with the tunnel located at the side of the excavation with a clearance of 25 mm (1.5 m in prototype), was used to provide results for comparisons with Case C. Elevated views of the two centrifuge tests are shown in Fig. 1b.

A square excavation (in plan) was carried out with dimensions of 300 × 300 mm (18 × 18 m in prototype). The depth of the excavation was 150 mm, equivalent to 9 m in the prototype. Excavation was modeled by drainage of a zinc chloride solution in front of the wall. All model tunnels were constructed from aluminum alloy with Young's modulus (E_a) of 70 GPa. The length, diameter, and thickness of the model tunnel are 1200, 100, and 3 mm, respectively. In the prototype, these dimensions are equivalent to 72, 6, and 0.18 m, respectively. All results presented in this study are at the prototype scale, unless stated otherwise, and details of centrifuge model packages and results can be found in [9].

Three-Dimensional Numerical Analysis

The finite-element program ABAQUS [13] was used to simulate the basement excavation. Figure 2a shows the 3D finite-element mesh adopted in the analyses, while Fig. 2b shows the layout of the monitored sections. The mesh was 1200 mm long, 750 mm high, and 990 mm wide. Eight-node brick elements were used to simulate sand and four-node shell elements were used to simulate both the tunnel and the diaphragm wall. Roller supports were applied on all vertical sides of the mesh, whereas pin supports were assigned to the base of the mesh. Therefore, movement normal to all vertical sides (x or y direction) and the movement in all directions (x, y, and z direction) at the base of the mesh were restrained.

A user-defined hypoplasticity soil model for granular material, as proposed by Von Wolffersdorff [14], was adopted in this paper. The advantages of the model are that it can reflect very basic features of soil behavior crucial for correct modeling of soil-structure interaction, such as nonlinear soil behavior, dependence of

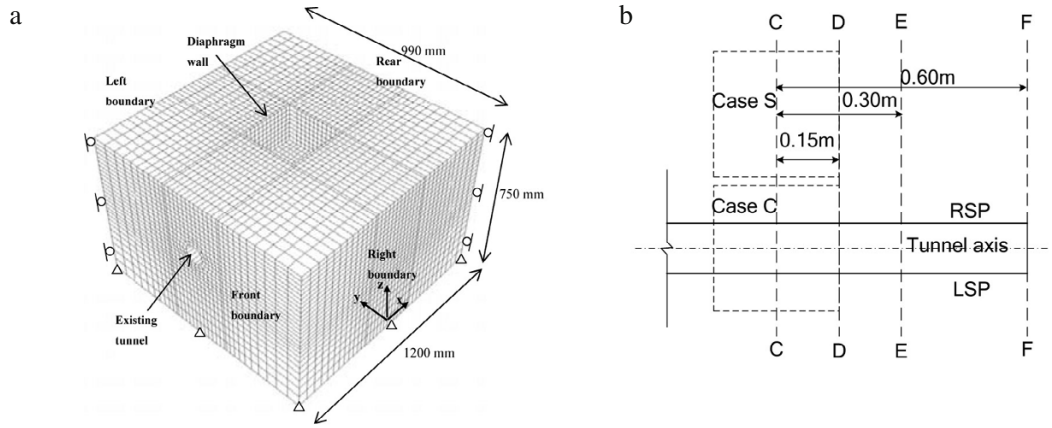

Fig. 2. Three-dimensional finite element mesh for case C (a) and layout of monitored sections (b) (model scale: 1:60).

stiffness on deformation history, and dependence of stiffness on stress level. Based on previous investigations, eight material parameters (critical state friction angle φ_c; granulates hardness h_s; exponents n, α, and β; minimum, critical, and maximum void ratio at zero pressure e_{d0}, e_{c0}, and e_{i0}) and another five soil parameters (parameters controlling the initial shear modulus upon 90° and 180° strain path reversal m_T and m_R, size of elastic range R, parameters controlling rate of degradation of stiffness with strain β_r and X) are needed to capture effects of strain and stress path dependence on soil stiffness [15]. Parameters for Toyoura sand in the reference model were obtained from Herle and Gudehus [16], while five parameters for intergranular strain were calibrated from a stiffness degradation curve [17, 18]. The lateral coefficient of earth pressure at rest $K_0 = 0.5$, $\varphi_c = 30^o$, $h_s = 2.6$ GPa, $n = 0.27$, $\alpha = 0.14$, $\beta = 3.0$, $e_{d0} = 0.61$, $e_{c0} = 0.98$, and $e_{i0} = 1.10$, $m_T = 4$ and $m_R = 8$, $R = 2\times10^{-5}$, $\beta_r = 0.1$ and X = 1.0, dry density $\rho_d = 1544$ kg/m^3, void ratio $e = 0.72$.

The tunnel lining and diaphragm wall were modeled as linear elastic materials, with Young's modulus and Poisson's ratio being set to 70 GPa and 0.2, respectively. The unit weight of the diaphragm wall was 27 kN/m^3. The numerical modelling procedure is the same as that in the centrifuge test. The excavation was divided into three steps: (1) establish the initial stress conditions, (2) incrementally increase gravitational acceleration of the whole model to 60 g, and (3) excavate the basement in 3 m rounds until the ultimate depth of the excavation is 9 m.

Comparison of Computed and Measured Results

To verify the numerical approach and provide a justifiable basis for extended analysis, some results from centrifuge model tests were compared with the numerical results. A comparison between measured and computed normalized tunnel vertical displacement at the crown along the tunnel axis is shown in Fig. 3. The results computed by numerical analysis are consistent with those measured in the centrifuge test, at least in terms of the trend. Vertical displacement of the tunnel crown increases with excavation depth, regardless of the approach. Within the zone of excavation ($x/(L/2) \leq 1$), tunnel heave was much larger than the zone outside the excavation ($x/(L/2) \geq 1$). A gentle heave trough appears beneath the excavation, with maximum vertical displacement of approximately 0.09% of the tunnel diameter (D) occurring at the C-C section (beneath the center of excavation). Comparison between the measured and computed results shows that the finite element analyses is effective and provides reasonable results. Extended numerical results, which cannot be obtained through centrifuge model tests, are discussed in the next section.

Deformation of the tunnel lining caused by excavation is shown in Fig. 4. The deformation is shown for both Cases C and S and the two sections C-C (center of the excavation) and D-D (edge of the excavation). In Fig. 4a, the maximum increase and reduction in tunnel radius (R) is 0.128% of R in a vertical direction and 0.125% of R in a horizontal direction in section C-C, respectively. In section D-D, the

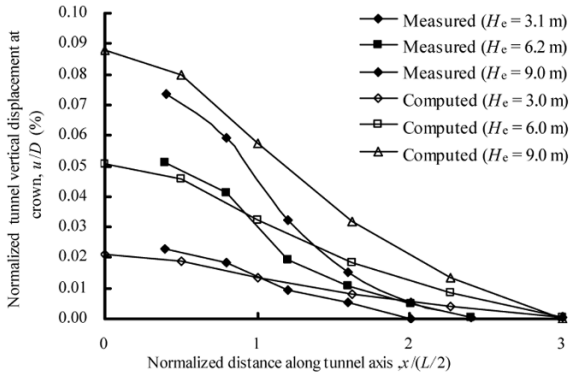

Fig. 3. Comparison of measured and computed normalized tunnel vertical displacement at the tunnel crown (measured data are reported by Ng et al. [9]).

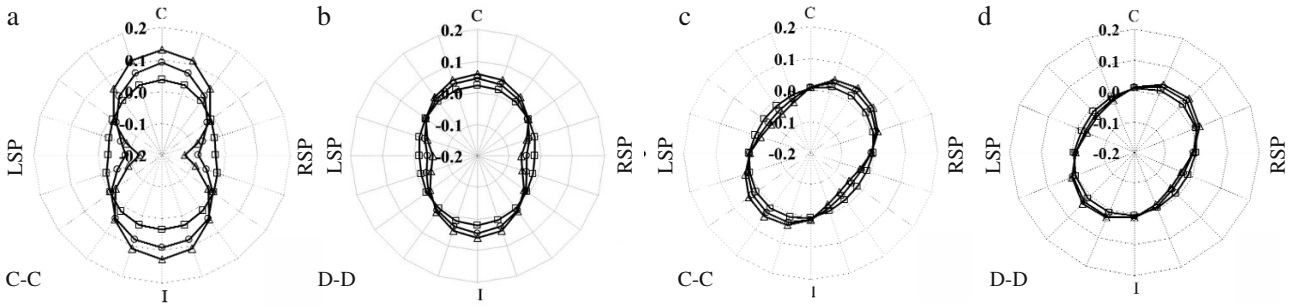

Fig. 4. Additional deformation of tunnel radius ($\Delta R/R$, %) in tunnel transverse section for: a and b) Case C; c and d) Case S); □) excavated to 3 m, ○) excavated to 6 m, and ∆) excavated to 9 m.

maximum increase and reduction in the tunnel radius is about 0.062% in a vertical direction and 0.055% in a horizontal direction. Thus, the tunnel is vertically elongated and horizontally compressed. However, the maximum increase and decrease in the tunnel radius in section C-C (Figs. 4c and d) is 0.055% in a subvertical direction and 0.052% in a subhorizontal direction. In section D-D, the maximum increase and decrease in the tunnel radius is 0.045% in a vertical direction and 0.038% in a horizontal direction. The existing tunnel is elongated along the connection between the right shoulder (RS) and left knee (LK) and compressed along the connection between the left shoulder (LS) and right knee (RK). The deformation mechanism is discussed later in terms of analysis of earth pressure distribution around the tunnel.

Comparison of the results for both sections shows that tunnel deformation changed dramatically from the center (section C-C) to the edge (section D-D), and one important implication of this uneven deformation of tunnel lining is the potential for differential movement of railways. As a consequence, trains traveling along such railways will rotate and twist along their axis, increasing the clearance requirements of the tunnel.

Normalized earth pressure distribution ($\Delta P/P_0$ in %) around the tunnel at various transverse sections during the excavation for Cases C and S is shown in Fig. 5, where P_0 denotes the initial earth pressure under gravity before excavation. For convenience, positive and negative signs denote an increase or decrease in earth pressure during excavation, respectively. It is evident that earth pressure decreases significantly in the center section of the basement (C-C section), but in section D-D, where the diaphragm wall is located, the maximum earth pressure increases greatly at the crown of the tunnel. The maximum earth pressure decreases from 60% in the D-D section to 4% of the initial earth pressure in the E-E section as the distance from the wall increases. Thus, the earth pressure at the center and edge sections of

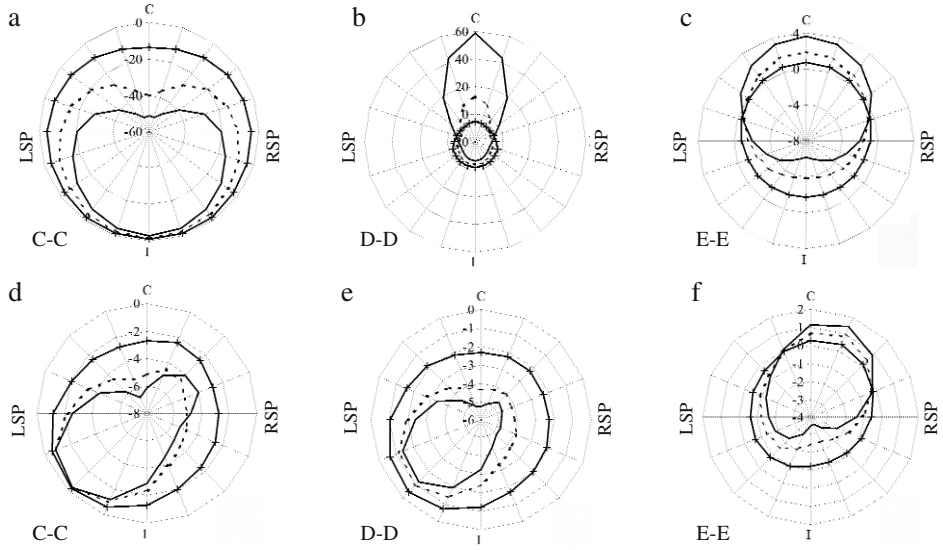

Fig. 5. Normalized earth pressure distributions ($\Delta P/P_0$ in %) around the tunnel at various transverse sections: a, b, and c) for Case C; d, e, f) for Case S; —+—) excavated to 3 m, **- - -**) excavated to 6 m, and ——) excavated to 9 m.

the excavation should be taken into account. Figure 5a shows that the normalized earth pressures around the tunnel decrease by 50% at the crown (C) and 20% at the springlines (SP) and show almost no change at the invert (I). The tunnel lining is elongated in the vertical direction and compressed in the horizontal direction because the earth pressure reduction at the crown is larger than the sum of reduction at the springlines (Fig. 4a). Figures 5b and c show that the normalized earth pressures around the tunnel increase at the crown but decrease at the springlines as the excavation advances. An obvious feature of the distribution shown in Fig. 5b is the sharp increase at the crown in section D-D. A possible reason for this is that the crown in section D-D acts as a support because of stress relief after excavation. It can be deduced that deformation at the crown is limited, which is consistent with the data shown in Fig. 4b. The change of normalized earth pressure in Case S (Fig. 5d-f) is much less than that for Case C. It is evident that the maximum changes in normalized earth pressure decrease by 7% near the crown, but change little at the LK around the tunnel after excavation. Similar distribution trends can also be found in section D-D (Fig. 5e). Figure 5f shows that the earth pressure increases at the RS during excavation, and the maximum decrease occurs around the invert as excavation advances. Based on the nonuniform distribution of earth pressure around the tunnel, it is evident that the tunnel lining elongates along a line connecting the RS and LK and compresses along a line connecting the LS and RK (Figs. 4c and d).

Changes in normalized total longitudinal, lateral, and vertical (x, y, and z directions) stresses with respect to their initial values ($\Delta\sigma_{xx}/(\sigma_{xx})_0$, $\Delta\sigma_{yy}/(\sigma_{yy})_0$, $\Delta\sigma_{zz}/(\sigma_{zz})_0$) for three soil elements (C, SP, and I) at section C-C are shown in Fig. 6a-c in terms of normalized distance ($x/(L/2)$) after excavation for Case C. Noticeable stress changes at the three selected elements take place within and at the edge of the excavation zone when the basement was excavated to 9 m. Within the excavation zone, stress reduction for each item ($\Delta\sigma_{xx}/(\sigma_{xx})_0$, $\Delta\sigma_{yy}/(\sigma_{yy})_0$, $\Delta\sigma_{zz}/(\sigma_{zz})_0$) is almost uniform. Significant stress increase in element C occurs at the edge of the basement, whereas there is no significant stress reduction or increase in other elements. The stress ratios at different elements recover to their initial condition as a result of longitudinal stress transfer. No further stress reduction is evident at distances from the center of the excavation of $3L/2$ for $\Delta\sigma_{xx}/(\sigma_{xx})_0$ and $5L/4$ for both $\Delta\sigma_{yy}/(\sigma_{yy})_0$ and $\Delta\sigma_{zz}/(\sigma_{zz})_0$, where L is the basement length.

In summary, the maximum stress reduction in the vertical direction takes place within the excavation zone, but the maximum stress increase occurs at the edge of the excavation. Similarly, both the

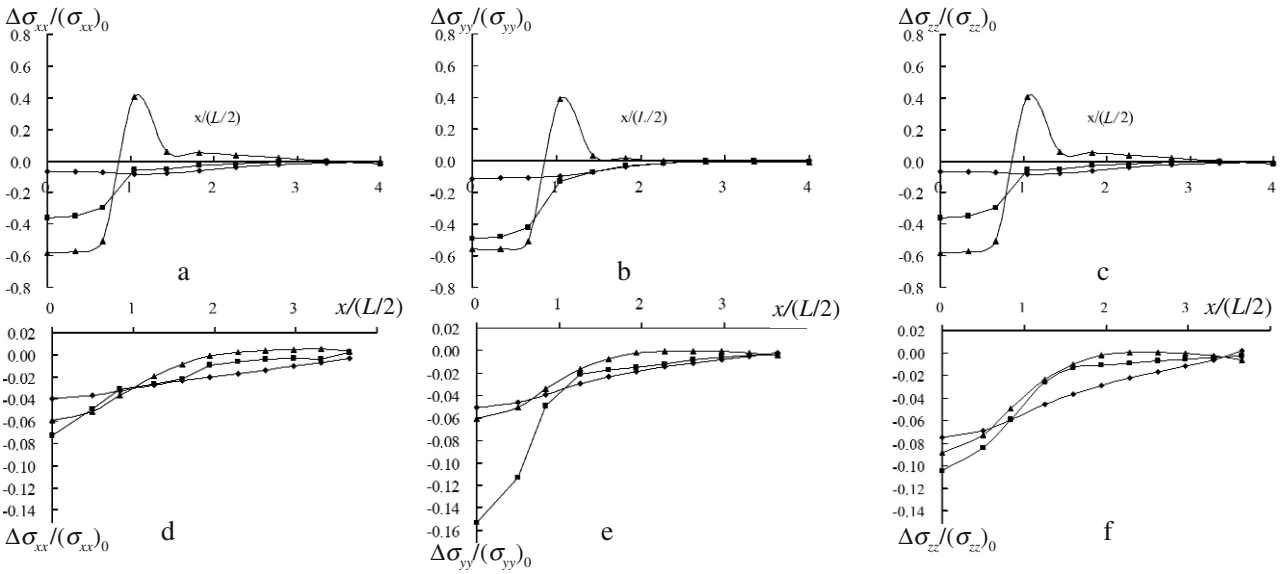

Fig. 6. Changes in normalized total longitudinal (a), lateral (b), and vertical (c) stress along the tunnel axis after excavation for Case C; and d, e, f) for Case S; ▲) crown C, ■) springline near the basement SP, and ◆) invert I.

maximum stress reduction in the lateral and longitudinal directions occurs in the excavation zone but with no significant stress change around the edge of the excavation. The maximum stress reduction in σ_{xx} and σ_{yy} are up to 60% of the initial stress value for all monitored elements, whereas the maximum stress reduction and increase in σ_{zz} are 75% and 40% of the initial stress values, respectively.

Changes in normalized total longitudinal, lateral, and vertical (x, y, and z directions) stresses with respect to their initial values ($\Delta\sigma_{xx}/(\sigma_{xx})_0$, $\Delta\sigma_{yy}/(\sigma_{yy})_0$, $\Delta\sigma_{zz}/(\sigma_{zz})_0$) for three soil elements (C, SP, and I) at section C-C are shown in Fig. 6d-f in terms of normalized distance ($x/(L/2)$) from section C-C after excavation in Case S. It is evident that imperceptible stress changes occur in the three selected elements along the tunnel axis, compared with Case C. Within the excavation zone, the absolute stress reduction for each item ($\Delta\sigma_{xx}/(\sigma_{xx})_0$, $\Delta\sigma_{yy}/(\sigma_{yy})_0$, $\Delta\sigma_{zz}/(\sigma_{zz})_0$) decreases gradually for all three elements, reaching a value of zero from section C-C at a distance of about $3L/2$. In the longitudinal and vertical directions there is no significant stress reduction along the tunnel axis, but some stress reduction occurs in the lateral direction. This is because more lateral earth pressure was released due to side excavation. Comparison of Figs. 6d-f shows that the patterns of stress change in the longitudinal, lateral, and vertical directions are similar, but the magnitudes of reduction for each individual element are different. After excavation, there is a maximum reduction of σ_{xx} of about 4%, 6%, and 7% at the invert, crown, and springline, respectively. There is a maximum reduction of σ_{yy} of 5%, 6%, and 15% at the I, C, and SP, respectively. Similar trends in maximum reduction of σ_{zz} are evident in Fig. 6f.

In summary, side excavation has little influence on stress changes in an existing tunnel. The maximum normal stress reduction occurs in the lateral direction, and accordingly, the maximum normal stress reduction for each element occurs at the springline, which is closest to the basement.

Conclusions

1. The distribution of tunnel lining deformation is symmetrical about the connection between crown and invert for Case C. The maximum increase of deformation related to excavation occurs at the crown or invert, while the maximum decrease occurs at the springlines. In Case S, the distribution of the tunnel lining deformation is symmetrical about the connection between the RS and LK. The maximum increase of deformation related to excavation occurs at the RS or LK, while the maximum decrease occurs at the LS and RK.

2. The reduction in earth pressure around the tunnel in the vertical direction (about 50%) is greater than that in the horizontal direction (about 20% at each springline) in Case C. The reduction in earth pressure in the RS-LK direction is greater than in the LS-RK direction in Case S. Therefore, the tunnel lining is vertically elongated and horizontally compressed in Case C, but elongated in the RS-LK direction and compressed in LS-RK direction in Case S.

3. The three-dimensional stress-transfer mechanism in soil elements around the tunnel is clearly demonstrated by changes in normal stresses (lateral, longitudinal, and vertical) caused by excavation. In Case C, the normal stress reduction (maximum 65%) is almost uniform within the excavation zone for all monitored elements, but there is a sharp stress increase (maximum 40%) at the edge of the crown of the excavation. In Case S, the side excavation has very little influence on stress changes in the existing tunnel. The maximum normal stress reduction (15%) occurs in the lateral direction. Accordingly, the maximum normal stress reduction for each individual element is at the springline, which is closest to the basement.

Acknowledgements

This study was sponsored by the National Natural Science Foundation of China (grant No. 51708245), the Natural Science Foundation of Jiangsu Province (No. BK20160426), and the National Natural Science Foundation of China (No. 51408254). We thank Warwick Hastie, PhD, from Liwen Bianji, Edanz Group China (www.liwenbianji.cn/ac), for editing the English text of a draft of this manuscript.

REFERENCES

1. D. Burford, "Heave of tunnels beneath the Shell Center, London, 1959-1986," Geotechnique, **38**(1), 135-137 (1988).
2. K. Y. Lo and J. A. Ramsay, "The effect of construction on existing subway tunnels – a case study from Toronto," *Tunn. Undergr. Sp. Tech*., **6**(3), 287-297 (1991).
3. M. Dolezalova, "Tunnel complex unloaded by a deep excavation," *Comput. Geotech*., **28**(6), 469-493 (2001).
4. J. S. Sharma, A. M. Hefny, J. Zhao, and C. W. Chan, "Effect of large excavation on displacement of adjacent MRT tunnels," *Tunn. Undergr. Sp. Tech*., **16**(2), 93-98 (2001).
5. G. Zheng and S. W. Wei, "Numerical analysis of influence of overlying pit excavation on existing tunnels," *J. Cent. South Univ. Technol.*, **15**(s2), 69-75 (2008).
6. H. L. Liu, P. Li, and J. Y. Liu, "Numerical investigation of underlying tunnel heave during a new tunnel construction," *Tunn. Undergr. Sp. Tech*., **26**(2), 276-283 (2011).
7. X. Huang, H. F. Schweiger, and H. W. Huang, "Influence of Deep Excavations on Nearby Existing Tunnels," *Int. J. Geomech*., **13**(2), 170-180 (2013).
8. J. W. Shi, C. W. W. Ng, and Y. H. Chen, "Three-dimensional numerical parametric study of the influence of basement excavation on existing tunnel," *Comput. Geotech*., **63**, 146-158 (2015).
9. C. W. W. Ng, J. W. Shi, and Y. Hong, "Three-dimensional centrifuge modelling of basement excavation effects on an existing tunnel in dry sand," *Can. Geotech. J*., **50**(8), 874-888 (2013).
10. C. W. W. Ng, J. W. Shi, D. Masin, H. S. Sun, and G. H. Lei, "Influence of sand density and retaining wall stiffness on three-dimensional responses of tunnel to basement excavation," *Can. Geotech. J*., **52**(11), 1811-1829 (2015).
11. X. Huang, H. W. Huang, and D. M. Zhang, "Centrifuge modeling of deep excavation over existing tunnels," *Geot. Eng*., **167**(1), 3-18 (2014).
12. C. W. W. Ng, H. S. Sun, G. H. Lei, J. W. Shi, and D. Masin, "Ability of three different soil constitutive models to predict a tunnel's response to basement excavation," *Can. Geotech. J*., **52**(11), 1685-1698 (2015).
13. ABAQUS, Inc., *ABAQUS User's and Theory Manuals*, Version 6.6, Providence Rhode Island, USA (2006).
14. P. A. Von Wolffersdorff, "A hypoplastic relationship for granular material with a predefined limit state surface," *Mech. Cohes-Frict. Mater*., **1**(3), 251-271 (1996).
15. A. Niemunis and I. Herle, "Hypoplastic model for cohensionless soils with elastic strain range," *Mech. Cohes-Frict. Mater*., **2**(4), 279-299 (1997).
16. I. Herle and G. Gudehus, "Determination of parameters of a hypoplastic constitutive model from properties of grain assemblies," *Mech. Cohes-Frict. Mater*., **4**(5), 461-486 (1999).
17. K. Maeda and K. Miura, "Confining stress dependency of mechanical properties of sands," *Soils Found*., **39**(1), 53-67 (1999).
18. S. Yamashita, M. Jamiolkowski, and D. C. F. Lo Presti, "Stiffness nonlinearity of three sands," *J. Geotech. Geoenviron. Eng*., ASCE, **126**(10), 929-938 (2000).